CORTICAL FLOW: INVESTIGATING THE SPATIOTEMPORAL DYNAMICS OF THE BRAIN

Julien Lefèvre[1,2,3], *Sylvain Baillet*[1,2]

[1]Cognitive Neuroscience & Brain Imaging Laboratory, CNRS–LENA, Paris, France
[2]UPMC Univ Paris 06, Paris, France
[3]Atomic Energy Commission (CEA), NeuroSpin Center, Saclay, France

ABSTRACT

Magneto- and Electro-Encephalography (MEG/EEG) offer probably the best trade-off between a superlative time resolution and a fair spatial one. At the scale of sensors, MEG/EEG signals reflect the global dynamic of the brain whereas sources imaging through inverse problem provide more regional behaviors. In both case, the data can be seen as spatiotemporal structures from which we can extract features such as optical flow, reflecting the amount of changes in the sequence of brain activations. After having recalled the theoretical basis of the so-called cortical flow, we present two applications in different experimental paradigms. We first show that our tool yields a temporal sequencing of brain events at a global scale. At last we focus on more local neural behaviors occurring in the visual cortex.

Index Terms— MEG, EEG, optical flow, brain dynamics, microstates

1. INTRODUCTION

Time-resolved functional neuroimaging using magneto (MEG) and electroencephalography (EEG) has now considerably matured and may report on the spatiotemporal dynamics of cortical activity at the millisecond range, with centimeter spatial resolution.

The MEG/EEG community has reported quite early that activation patterns at the surface of the head revealed kind of landscape changes or less metaphorically quasi continuous evolutions [1]. Analysis of such evolutions have often favored geometrical approaches where MEG/EEG signals are represented by a trajectory in a high dimensional space [2]. This method allowed first to suggest a quantitative description of so-called brain microstates. However this viewpoint fails to describe precisely the local spatiotemporal structure of dynamical changes.

In other domains such as meteorology, tools from the computer vision community have been used to identify and track specific patterns of physical phenomena evolving in both space and time – e.g. cloud ensembles [3] and aurora borealis [4] – using optical flow techniques derived from the seminal work by Horn and Schunck [5].

In this paper, we first recall a new method that yields the optical flow of brain activations computed onto the complex cortical geometry. We also describe how this tool might be aplied beneficially to the elucidation of some aspects of mass neural dynamics both at the global and regional scales.

2. METHODS

2.1. The concept of cortical flow

We have recently introduced the concept of cortical flow [6] to characterize the dynamics of spatially-distributed brain activations at a spatial scale accessible to MEG/EEG brain mapping; i.e. on the order of 1 cm. Under the assumption that the continuous distribution of neural activity $I(p,t)$ has been obtained in space and time from MEG/EEG data inverse modeling, a vector field $\mathbf{V}(p,t)$ might be derived at each point p of the cortical manifold, which reflects the local displacements of patterns of neural activation with time t. Under the seminal hypothesis of the conservation of intensity I, this vector field or *optical flow* satisfies :

$$\partial_t I + \mathbf{V} \cdot \nabla_{\mathcal{M}} I = 0. \quad (1)$$

Note that the scalar product is modified by the local curvature of $\mathcal{M}$, the domain of interest which is typically the cortical surface.

2.2. Computation

2.2.1. Theory

The solution to Eq. 1 is not unique as long as the components of $\mathbf{V}(p,t)$ orthogonal to $\nabla_{\mathcal{M}} I$ are left unconstrained. This so-called 'aperture problem' has been addressed by a large number of methods using e.g. regularization approaches. These latter may be formalized as the minimization problem of an energy functional, which both includes the regularity of the solution and the agreement to the model:

$$\mathcal{E}(\mathbf{V}) = \int_{\mathcal{M}} \left[\frac{\partial I}{\partial t} + \mathbf{V} \cdot \nabla_{\mathcal{M}} I \right]^2 \mathrm{d}\mu + \lambda \int_{\mathcal{M}} \mathcal{C}(\mathbf{V}) \mathrm{d}\mu. \quad (2)$$

Here we have considered $\mathcal{C}(\mathbf{V})$ as a regularity factor which operates quadratically on the gradient of the expected vector field:

$$\mathcal{C}(\mathbf{V}) = \mathrm{Tr}({}^t\nabla\mathbf{V}.\nabla\mathbf{V}), \tag{3}$$

where Tr is the trace operator. It extends the seminal model of Horn and Schunck [5] in which the domain of interest $\mathcal{M}$ is equal to $\mathbb{R}^2$. In this particular case the regularizing term reads :

$$\mathcal{C}(\mathbf{V}) = \left(\frac{\partial V_x}{\partial x}\right)^2 + \left(\frac{\partial V_x}{\partial y}\right)^2 + \left(\frac{\partial V_y}{\partial y}\right)^2 + \left(\frac{\partial V_y}{\partial x}\right)^2 \tag{4}$$

Both for 2D images [7] and more general problems on surfaces [6], minimization of (2) reduces to finding a vector field $\mathbf{V}$ satisfying:

$$a(\mathbf{V}, \mathbf{U}) = f(\mathbf{U}), \tag{5}$$

for any $\mathbf{U}$ belonging to some subspace of smooth vector fields. a and f consists of a bilinear symmetric definite positive form and a linear form of $\nabla_{\mathcal{M}} I$.

2.2.2. Numerical aspects

We have recently suggested an approach based on the finite elements method (FEM) [8] to address the problem introduced in Section 2.2.1 [6]. We have demonstrated that this strategy is relevant and efficient when considering solving this problem on surface tessellations as irregular as the brain's. The basic idea consists in writing the unknown vector field as a linear combination of the basis functions $(\mathbf{W}_{i,\alpha})_{i=1:N,\alpha=1:2}$, which are elementary vector fields defined at the N nodes of the surface mesh of interest.

From (5), the coefficients – $x_{j,\beta}$ – of $\mathbf{V}$ expressed in this basis are solutions of the linear problem:

$$\sum_{j=1:N,\beta=1:2} a(\mathbf{W}_{i,\alpha}, \mathbf{W}_{j,\beta}) x_{j,\beta} = f(\mathbf{W}_{i,\alpha}), \tag{6}$$

for $i = 1 : N$ and $\alpha = 1 : 2$. Thus a simple inversion of the symmetric, definite, positive matrix $[a(\mathbf{W}_{i,\alpha}, \mathbf{W}_{j,\beta})]$ yields a regularized estimate of the optical flow over any arbitrary surface manifold.

2.3. Investigation of brain global dynamics

2.3.1. Sequencing time-resolved functional image series

From the local directionality measures on brain activations as conveyed by $\mathbf{V}(x,t)$, we were interested in instantiating a quantitative index reflecting the global spatiotemporal changes at every instant of a given time sequence of neural activities. We define the global displacement energy (DE) of neural activations as an analogue to a kinetic energy:

$$DE(t) = \int_{\mathcal{M}} \| \mathbf{V} \|^2 \ \mathrm{d}\mu. \tag{7}$$

The larger $DE(t)$, the more likely the global topography of brain activations is undergoing large scale changes. Conversely, the smaller $DE(t)$, the more likely it is installed in a semi-stable episode. Hence we revisit the concept of brain stable microstates and redefine their occurrence as local minimal basins of $DE(t)$.

2.3.2. Analysis of brain microstates at the group level

We now introduce a method to investigate the reproducibility of the temporal sequencing defined in 2.3.1 at the level of a group of subjects. Let us consider a study involving n_s subjects and call $(t_i^s)_{i=1\ldots n_s}$ the time instants when $DE_s(t)$ reaches a local minimum for subject s. Finally, we define $(\mathbf{I}_i^s)_{i=1\ldots n_s}$ as the set of n_s corresponding activities. We follow the steps :

- Sorting the big vector composed of all the values (t_i^s). Calling $\mathbf{T}$ the sorted vector, we compute

$$dt_{max} = \max\left\{\mathbf{T}_{j+1} - \mathbf{T}_j\right\}$$

- Segmentation of the considered temporal period in contiguous intervals whose length is at most dt_{max}. Definition of the sets T_n^s corresponding to the temporal instants (t_i^s) belonging to the nth previously defined interval.

- Definition of the sets [1]

$$E_{m,n} = \left\{ Corr\left(\mathbf{I}_i^s, \mathbf{I}_{i'}^{s'}\right) / \exists(s,s'),\ i \in T_m^s,\ i' \in T_n^{s'} \right\}$$

  where $Corr$ is the classical Pearson correlation applied to the two spatial configurations.

- Construction of a (symmetric) matrix encoding the possible similarity between neural activities taken from different subjects and possibly different time periods. Its coefficients are given by

$$\mu_{m,n} = Mean(E_{m,n})$$

  corrected by a last normalization step using Z-score with respect to a pre-stimulation period :

$$Z_{m,n} = \frac{\mu_{m,n} - Mean(\cup_{m,n \in baseline} E_{m,n})}{\sqrt{Var(\cup_{m,n \in baseline} E_{m,n})}}$$

3. RESULTS

3.1. Data

We have used two different experimental protocols in Magnetoencephalography in order to study the spatiotemporal dynamic of the brain at global and local scales. The first one is

[1] They are not empty by definition of dt_{max}.

a pure visual stimulation of an expending checkerboard rings (Fig. 1) at the frequency of 5 Hz, known to produce steady state activities in localized parts of the brain, such as visual areas [9]. In the second one a subject sees a ball falling and has to catch it (condition A) or not (condition B) [10]. In this task the brain is supposed to come across different steps from the perception of the objects to the coordination and anticipation and at last the catching which occurs around 400 ms.

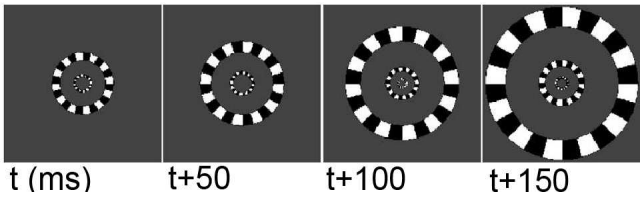

Fig. 1. Expanding checkerboards at 5 Hz in a pure visual stimulation.

3.2. Global behavior

We applied the method exposed in 2.3.2 in order to describe different brain states in the ball-catching task. On Fig. 2 are plotted the matrices $Z_{m,n}$ for the two experimental conditions. The considered temporal window ($[-0.5, 0.6]$s, restrained for convenience purpose) has been divided in 50 intervals (dt_max equals 58 in the catch condition and 54 in the nocatch).

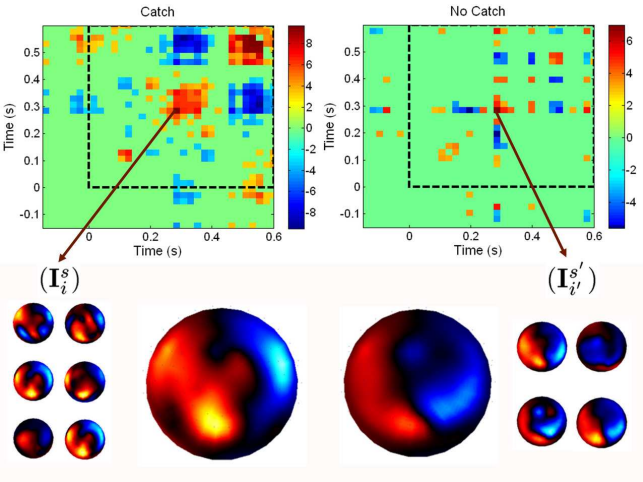

Fig. 2. First line : matrices $[Z_{m,n}]$ for each experimental condition. The dotted square indicates the time period during which the subjects are performing the task. Second lines : left (resp. right), 6 (resp. 4) MEG topographies associated to a temporal interval around 300 ms and the averaged topography.

The visual inspection of the matrices allows first to qualitatively distinguish the two conditions: For example there is a huge red pattern between 300 and 400 ms in the catch condition only. It reflects a best correlation between the topographies of stable MEG activations with respect to the prestimulus period. This suggests the existence of a strong reproducibility during this time period which could correspond to the motor preparation.

Moreover if we examine precisely a small temporal interval around 300 ms (the red one indicated by the arrows on both images) we can extract the 6 (resp. 4) corresponding topographies (called $\mathbf{I}_i^s$ in 2.3.2) and the averaged topography in the catch (nocatch) condition. The comparison of the two averaged topographies shows immediately spatial differences between the two conditions.

3.3. Local directionality of neural information

On Fig. 3 we show a part of the left hemisphere and brain activations (in slight red color) during the pure visual stimulation at different time steps. More precisely the region of interest corresponds to the occipital lobe which is well-known to contain the visual areas [11].

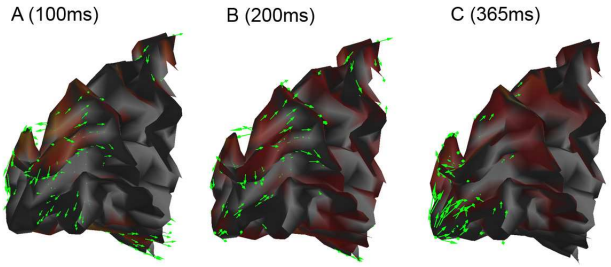

Fig. 3. Sagittal view of the left occipital lobe : optical flow (green) at several instants. The reconstructed MEG activities are shown in a slight red shade.

We have plotted the optical flow of the MEG activations with green arrows. However this representation is purely illustrative and provides a lot of supplementary information. Thus we propose an alternative visualization of this flow in space and time on Fig. 4.

We consider a point p located in the calcarine sulcus (yellow) where the norm of the optical flow is maximum across the time. We display the trajectory of this vector in the tangent plane of p when the time is varying. According to [9], we can separate the considered temporal window in three intervals : the baseline ($[-0.5, 0]$, green), the transitory regime ($[0, 0.4]$, blue) and the stationary regime ($[0.4, 1.5]$, red). We can note that after the transitory period the optical flow trajectory seems to follow an ellipsoid shape. It can be compared to a limit cycle, which is a type of attractor in the dynamical system framework.

At last it is interesting to compare the geometry of the flow trajectory and the underlying cortical geometry : the principal axis of the red ellipse has the same orientation as the calcarine

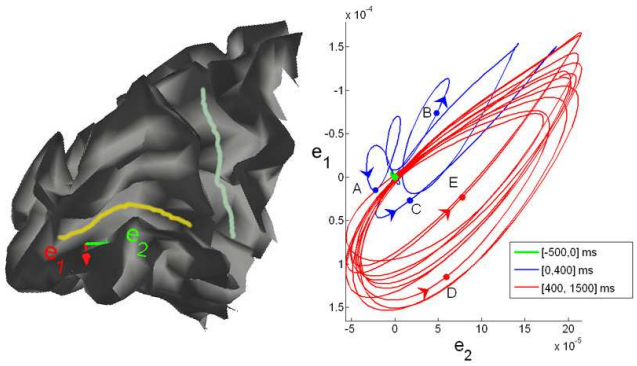

Fig. 4. Left : sagittal view of occipito-parietal lobe of the left hemisphere. Calcarine sulcus (yellow) and parieto-occipital sulcus (blue). $\mathbf{e}_1$ and $\mathbf{e}_2$ are basis vectors of the tangent plane at a point p where the norm of flow vector is maximal. Right : Trajectory of the flow vector in the tangent plane $(p, \mathbf{e}_1, \mathbf{e}_2)$. The different colors correspond to different time periods (see text).

sulcus. In other terms the expansion of the rings seems to be correlated to propagations along the calcarine. This result confirms retinotopic studies [11] and suggests that a dynamical retinotopy could also be investigated through MEG and optical flow analysis.

4. CONCLUSION

We have proposed two applications of the cortical flow, a tool adapted from computer vision community. In the first one we have seen that the global brain dynamic come across some reproducible events at the group level. Moreover our analysis allows to distinguish clear qualitative effects between two experimental conditions. The second application demonstrates that optical flow provides relevant indices of directionality in visual areas in accord with previous retinotopic studies. Thus cortical flow could reflect the local flow of neural information.

After these encouraging results, we plan to investigate the robustness of the global approach through other cognitive tasks and to enrich the local description of optical flow by connectivity indices between distant brain areas.

5. REFERENCES

[1] D. Lehmann and W. Skrandies, "Spatial-analysis of evoked-potentials in man: a review," *Progress in neuroboiology*, vol. 23, no. 3, pp. 227–250, 1984.

[2] R.D. Pascual-Marqui, C.M. Michel, and D. Lehmann, "Segmentation of brain electrical activity into microstates: Model estimation and validation," *IEEE Trans. Biomed. Eng.*, vol. 42, pp. 658–665, 1995.

[3] T. Corpetti, E. Mmin, and P. Prez, "Dense estimation of fluid flows," *IEEE Transactions on Pattern Analysis and Machine Intelligence*, vol. 24, no. 3, pp. 365–380, March 2002.

[4] EM Blixt, J. Semeter, and N. Ivchenko, "Optical flow analysis of the aurora borealis," *Geoscience and Remote Sensing Letters, IEEE*, vol. 3, no. 1, pp. 159–163, 2006.

[5] B.K.P. Horn and B.G. Schunck, "Determining optical flow," *Artificial Intelligence*, vol. 17, pp. 185–204, 1981.

[6] J. Lefèvre, G. Obozinski, and S. Baillet, "Imaging brain activation streams from optical flow computation on 2-riemannian manifold," *Proc. Information Processing in Medical Imaging*, pp. 470–481, 2007.

[7] C. Schnorr, "Determining optical flow for irregular domains by minimizing quadratic functionals of a certain class.," *Int. J. Computer Vision*, vol. 6(1), pp. 25–38, 1991.

[8] P.G. Ciarlet, *Finite Element Method for Elliptic Problems*, Society for Industrial and Applied Mathematics Philadelphia, PA, USA, 2002.

[9] D. Cosmelli, O. David, J.P. Lachaux, J. Martinerie, L. Garnero, B. Renault, and F. Varela, "Waves of consciousness: ongoing cortical patterns during binocular rivalry," *Neuroimage*, vol. 23, no. 1, pp. 128–140, 2004.

[10] P. Senot, M. Zago, F. Lacquaniti, and J. McIntyre, "Anticipating the effects of gravity when intercepting moving objects: Differentiating up and down based on nonvisual cues," *J Neurophysiol*, vol. 94, pp. 4471–4480, 2005.

[11] B.A. Wandell, "Computational neuroimaging of human visual cortex," *Annual Review of Neuroscience*, vol. 22, no. 1, pp. 145–173, 1999.